PLOS ONE

RESEARCH ARTICLE

Higher vascularity at infiltrated peripheral edema differentiates proneural glioblastoma subtype

Eduard Chelebian[1,2]*, Elies Fuster-Garcia[3], María del Mar Álvarez-Torres[1], Javier Juan-Albarracín[1], Juan M. García-Gómez[1]

1 Instituto Universitario de Tecnologías de la Información y Comunicaciones, Universitat Politècnica de València, València, Spain, **2** Department of Information Technology, Uppsala University, Uppsala, Sweden, **3** Department of Diagnostic Physics, Oslo University Hospital, Oslo, Norway

* edchekoc@etsii.upv.es

Citation: Chelebian E, Fuster-Garcia E, Álvarez-Torres MdM, Juan-Albarracín J, García-Gómez JM (2020) Higher vascularity at infiltrated peripheral edema differentiates proneural glioblastoma subtype. PLoS ONE 15(10): e0232500. https://doi.org/10.1371/journal.pone.0232500

Editor: Thomas Pyka, Technische Universitat Munchen, GERMANY

Received: April 12, 2020

Accepted: September 29, 2020

Published: October 14, 2020

Data Availability Statement: Data is available from TCGA-GBM public repository: http://doi.org/10.7937/K9/TCIA.2016.RNYFUYE9. All relevant data are within the manuscript and its Supporting Information files.

Funding: This work was partially supported by: MTS4up project (National Plan for Scientific and Technical Research and Innovation 2013-2016, No. DPI2016-80054-R) (JMGG); H2020-SC1-2016-CNECT Project (No. 727560) (JMGG), Fundació Bancaria laCaixa (LCF/TR/CI16/10010016) and

Abstract

Background and purpose

Genetic classifications are crucial for understanding the heterogeneity of glioblastoma. Recently, perfusion MRI techniques have demonstrated associations molecular alterations. In this work, we investigated whether perfusion markers within infiltrated peripheral edema were associated with proneural, mesenchymal, classical and neural subtypes.

Materials and methods

ONCOhabitats open web services were used to obtain the cerebral blood volume at the infiltrated peripheral edema for MRI studies of 50 glioblastoma patients from The Cancer Imaging Archive: TCGA-GBM. ANOVA and Kruskal-Wallis tests were carried out in order to assess the association between vascular features and the Verhaak subtypes. For assessing specific differences, Mann-Whitney U-test was conducted. Finally, the association of overall survival with molecular and vascular features was assessed using univariate and multivariate Cox models.

Results

ANOVA and Kruskal-Wallis tests for the maximum cerebral blood volume at the infiltrated peripheral edema between the four subclasses yielded false discovery rate corrected p-values of <0.001 and 0.02, respectively. This vascular feature was significantly higher ($p = 0.0043$) in proneural patients compared to the rest of the subtypes while conducting Mann-Whitney U-test. The multivariate Cox model pointed to redundant information provided by vascular features at the peripheral edema and proneural subtype when analyzing overall survival.

Conclusions

Higher relative cerebral blood volume at infiltrated peripheral edema is associated with proneural glioblastoma subtype suggesting underlying vascular behavior related to molecular composition in that area.

H2020-SC1-BHC-2018-2020 (No. 825750) (JMGG); PID2019-104978RB-I00 (Ministerio de Ciencia e Innovación) (JMGG). MAT was supported by DPI2016-80054-R (Programa Estatal de Promoción del Talento y su Empleabilidad en I+D +i). EFG was supported by the European Union's Horizon 2020 research and innovation program under the Marie Skłodowska-Curie grant agreement No 844646. There was no additional external funding received for this study.

Competing interests: The authors have declared that no competing interests exist.

Introduction

In the late years, Central Nervous System tumor classification has shifted from being based on microscopic similarities between cells and their levels of differentiation [1] to additionally include genetic-based features [2]. This is particularly the case for glioblastoma, where several classifications have been defined: on the one hand, the World Health Organization (WHO) classification which distinguishes between *IDH*-wildtype and *IDH*-mutant glioblastomas [2–4] and, on the other, the Verhaak classification [5], consisting of 4 subtypes depending on mutations and molecular profile of various cancer-related genes. These subtypes are the mesenchymal, classical, neural and proneural, the latter being related to *IDH* mutations [5, 6]. These new classification paradigms have improved the estimation of prognosis [7, 8] and proposed specific therapeutic targets [9–12], especially for patients with proneural and mesenchymal type glioblastoma.

Considering that Magnetic Resonance Imaging (MRI) perfusion biomarkers have been associated with patients' overall survival [13–15] and cellular features [16, 17], several studies were performed to analyze if there was a relationship between vascular biomarkers and the genomic subtypes classifications. Barajas *et al*. studied the influence of glioblastoma genetic and cellular features over MRI, concluding that they could spot the most malignant regions within the tumor [18]. Jain *et al*. demonstrated that combining Verhaak subtypes with vascularity markers at the enhancing tumor provides additional information as a survival predictor [19]. However, they found that the enhancing and non-enhancing regions of the tumor did not present any significant correlations with the genomic subclassification. Another study proposed that tumor blood volume determined by dynamic susceptibility contrast MR perfusion imaging was related to *EFGR* and to *PTEN* expression in some patients [20].

Most of these studies focus on the vascularity of the enhancing tumor region and only a few remarked the influence of the non-enhancing part of the tumor including the edema region [18, 20]. Gill *et al*. [21] found molecular differences between Verhaak subtypes performing MRI-localized biopsies in the peripheral edema region. Similarly, Price *et al*. [22] discovered that metabolic and perfusion changes in this region could be found using multimodal MR images. In this sense, we hypothesize that the vascular parameters in the invasive margins of glioblastoma could be related to characteristic combinations of mutations.

The purpose of this article is to assess the correlation between the vascularity present at the infiltrated peripheral edema habitat at preoperative stage and Verhaak molecular classification. To do so, we propose the use of a multicentrically validated [23] automatic open service named ONCOhabitats (https://www.oncohabitats.upv.es) proposed by Juan-Albarracín *et al*. [15, 24, 25]. To ensure the comparability of our study, the analysis was performed on the TCGA-GBM open database [26], which contains MR images and molecular information. In the end, we found correlation between peripheral edema vascularity and specially the proneural glioblastoma subtype.

Materials and methods

Patient selection

Our study included retrospective patients with glioblastoma from The Cancer Imaging Archive—TCGA-GBM [26], an open dataset which only uses anonymized data, available at: https://wiki.cancerimagingarchive.net/display/Public/TCGA-GBM (Version 3). The database consists of 262 histopathological validated glioblastoma patients, 66 of which had preoperative dynamic susceptibility contrast enhanced T2*-weighted perfusion (DSC) imaging information. Three of them were excluded because they did not have genomic information available.

The remaining 63 belong to two different institutions with the following distribution: 48 in the first and the rest in the second. From the first institution, 6 were excluded because of poor perfusion acquisition, mainly due to having an incomplete field of view in the DSC images. Additionally, 5 were excluded due to post-processing errors when performing DSC quantification. From the second one, only 2 were not considered for having an incomplete FOV.

The final cohort was made up of 50 primary glioblastoma patients who had all underwent tumor resection. Age distribution (mean years [minimum, maximum]) was: 13 females (55.2 years [17, 74]) and 37 males (59.5 years, [17, 81]); overall (58.4, [17, 81]). Additionally, IDH mutation status was available for 39 patients, from which only one was IDH-mutated. MGMT methylation status was available for 10 patients, from which only two were MGMT-methylated.

According to the Verhaak molecular classification [27, 28], the group of patients would be divided into 10 classical, 17 mesenchymal, 11 neural and 12 proneural subtype glioblastomas, attending to the mutations and markers they presented. The cohort clinical and genetic data along with the subtype of each subject can be found in the S1 Table, whose complete information is retrieved from the original at the TCGA-GBM website [26].

MRI imaging acquisition

From both institutions only 17 studies were obtained using 3T magnetic resonance imaging machines, all belonging to the first institution. For the rest of them, 1.5T imagers were used.

DSC perfusion MRI was performed during the injection of the gadolinium-based contrast (0.1 mmol/kg) using 95 dynamics for the first institution and 60 dynamics for the second institution of $T2^*$-weighted gradient echo echoplanar images. T1, T2 and fluid attenuation inversion recovery (FLAIR) MR images were acquired before the DSC perfusion. Gadolinium enhanced T1-weighted (T1-Gd) images were obtained after. The acquisition matrices were either 128x128 or 256x256, with slice thicknesses ranging from 1.5 to 6.0 mm. S2 Table shows repetition time (ms) / echo time (ms) / flip angle (°) of the acquisitions for every patient.

Computing vascular habitats

All the cases were processed using the Hemodynamic Tissue Signature service found in the ONCOhabitats platform [24]. It provides a reproducible [23] and automated methodology to define habitats withing the glioblastoma, based on the vascular properties of the lesion, as shown in Fig 1.

Morphological sequences are used for segmentation of enhancing tumor and edema. The resulting segmentation together with DSC perfusion maps are used to obtain the vascular habitats.

The methodology consists of 4 stages: 1) MRI preprocessing, 2) DSC perfusion quantification, 3) glioblastoma tissue segmentation, and 4) vascular habitats detection.

MRI preprocessing includes several modules for denoising, inhomogeneity correction, registration, brain extraction, motion correction or intensity standardization.

DSC perfusion maps are calculated following standard methods published in the literature. The block-circulant SVD decomposition method and numerical integration of gamma-variate concentration-time curves are used to estimate rCBF and rCBV respectively. Boxerman leakage correction method [29] is also employed to correct for T1- and T2-extravassation effects.

Glioblastoma tissue segmentation is performed through a Convolutional Neural Network (CNN) trained with more than 300 cases manually segmented by several expert radiologists. The CNN works with 3D MRI patches of post-Gadolinium T1-weighted, T2-weighted and FLAIR images. The network follows a U-net architecture with skip-connections and residual-inception blocks, achieving a Dice performance in whole tumor segmentation of 0.90 [30].

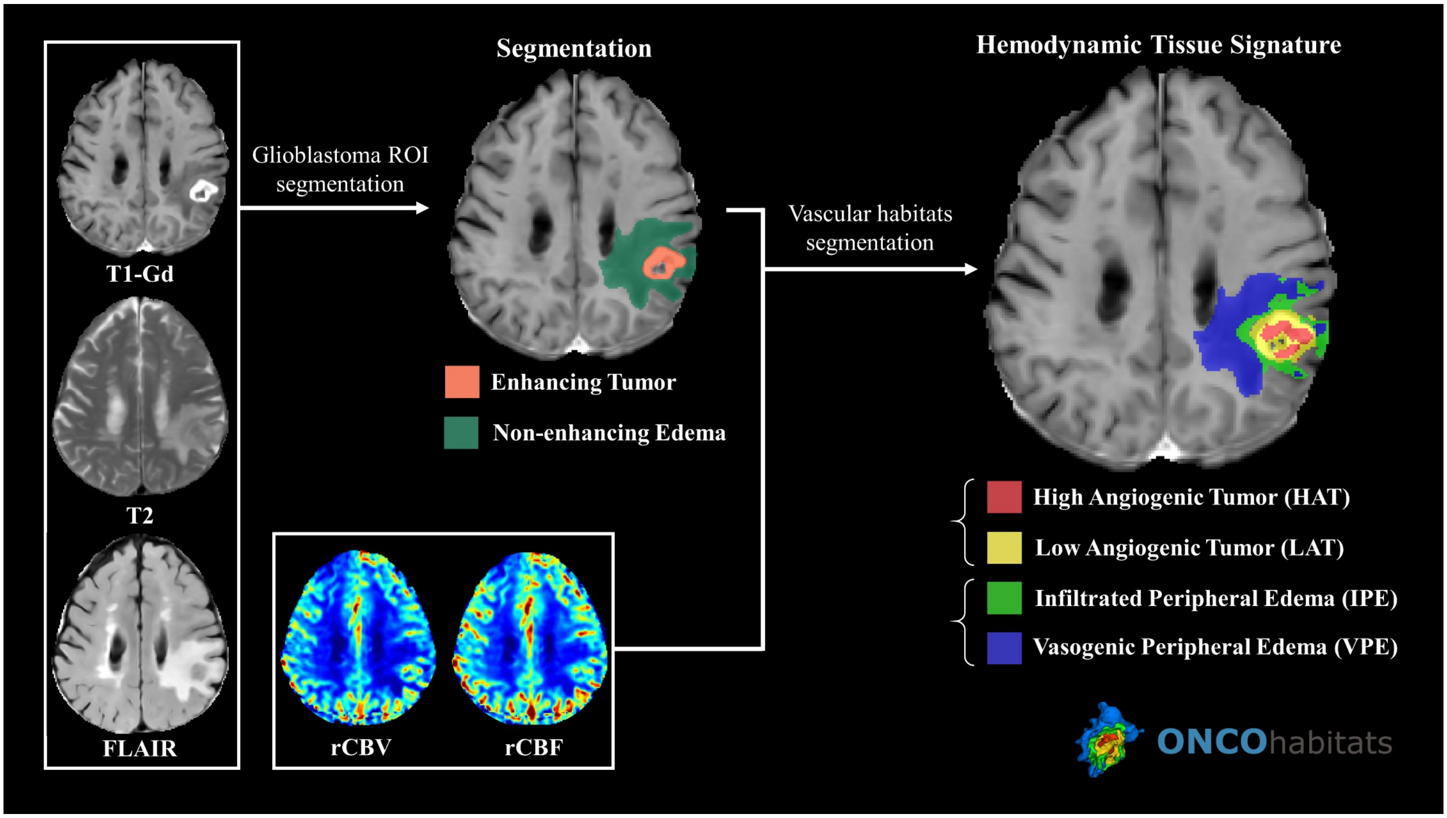

Fig 1. Hemodynamic Tissue Signature pipeline in ONCOhabitats.

https://doi.org/10.1371/journal.pone.0232500.g001

Vascular habitats are obtained through an unsupervised methodology based on NL-SVFMM [31] method. A mixture of 4 classes is fit into the region delineated by the morphological segmentation of the enhancing tumor and edema to obtain the habitats. Several physiological constraints are introduced during the clustering process to drive the segmentation to a physically plausible delineation of the habitats. For the case of the IPE habitat, which is the relevant habitat studied in this work, their apparition is constrained, following the specifications of Guo *et al.* [32], to a 2 cm margin around the enhancing tumor, which is considered the plausible region where edema could be infiltrated by the tumor. The remaining habitats, that is, the high angiogenic tumor (HAT), low angiogenic tumor (LAT) and the vasogenic peripheral edema (VPE), also introduce constraints limiting their locations and proportions of occurrence within the lesion.

$rCBV_{max}$, $rCBV_{mean}$ and $rCBV_{median}$ were calculated for each vascular habitat. $rCBV_{max}$ was defined as the 95th percentile of the distribution of rCBV values within the ROI in order to increase robustness. Values of $rCBV_{max}$, $rCBV_{mean}$ and $rCBV_{median}$ at each habitat for each subject are presented in the S3 Table.

Statistical analysis

Firstly, ANOVA and Kruskal-Wallis H test were performed at the ET -in order to have comparable results with the current literature-, consisting of HAT and LAT regions, and at the IPE using all perfusion parameters ($rCBV_{max}$, $rCBV_{mean}$ and $rCBV_{median}$) across Verhaak subclasses. This will serve as a first approximation for establishing any significant divergences in vascularity values regarding the Verhaak subtypes.

For deepening the analysis on the specific differences between the four subclasses, Wilcoxon–Mann–Whitney tests were executed in each habitat. The comparison was made between classical, mesenchymal, neural and proneural classes individually one against the other, and comparing each one of them against the three remaining. For significant experiments, ROC curves were drawn for threshold optimization.

These statistical tests were considered significant when p-values were under 0.05. To correct for multiple testing, Benjamini-Hochberg false discovery rate correction was carried out for every study. Analyses were carried out on a personal computer with MATLAB R2018a (Natick, Massachusetts, USA).

Finally, survival Cox proportional hazards analysis were carried out in order to assess the effect of Verhaak subtypes on Cox overall survival models based only on perfusion parameters. To this end, univariate survival models were fitted using only $rCBV_{max}$ at IPE and at ET. Then, univariate models using only each subtype were fitted. Finally, multivariate models with both $rCBV_{max}$ and each subtype as cofactor were studied. The consequences of subtype addition can be either worsening or improving the fitting, indicating that the subtype provides redundant information or not, that is, there is an association between subtype and vascularity at IPE or not.

For each Cox model, Hazard Ratio (HR) with 95% confidence intervals (CI95), area under ROC curve (AUC) and p-values are reported. Significance will be considered when p-values are under 0.05. Analyses were carried out on a personal computer using R statistical analysis software [33].

Results

Verhaak subtypes and rCBV in vascular habitats

In Fig 2 the Box-Whiskers representation of $rCBV_{max}$ values at the vascular habitats for each Verhaak subtype is represented. Firstly, as expected, a decrease in vascularity can be observed as we move from HAT to VPE. The proneural subtype shows higher vascularity in every habitat. However, there is important overlap at the enhancing areas, whereas at IPE and, to a lesser degree, at VPE the difference with the rest of the subtypes is bigger. This may point to vascularity differences in the peripheral region.

These results are consistent with the ones presented in Table 1. rCBV values at the ET were not significantly different among Verhaak subclasses neither performing an ANOVA nor a Kruskal-Wallis test. However, performing the same analyses on the IPE, significance is found for every rCBV metric (i.e. Max, Mean, Median).

Proneural subtype differences in rCBV at IPE region

Fig 3 shows the mean rCBV at IPE distribution density for each subtype in solid line and dotted lines represent each patient's rCBV distribution densities at IPE. Subtypes for both mean and individual distributions are represented by different colors. An important difference can be seen in the proneural subtype vascularity distribution, explaining the global differences found in the previous section.

Results of subtype-specific tests at IPE are presented in Table 2. Comparing $rCBV_{max}$ values at the IPE habitat between the Verhaak subtypes, we obtained that the proneural tumor subtype has a significantly differentiated peritumoral vascularity. Note that the most significant difference was found between proneural and mesenchymal subtype. Mesenchymal subtype vascularity was significantly different from the other three subtypes only before multiple-test correction. Classical and neural subtypes had indistinguishable vascularity at the IPE according to this test, both one from the other and the two from the other subtypes. The same tests

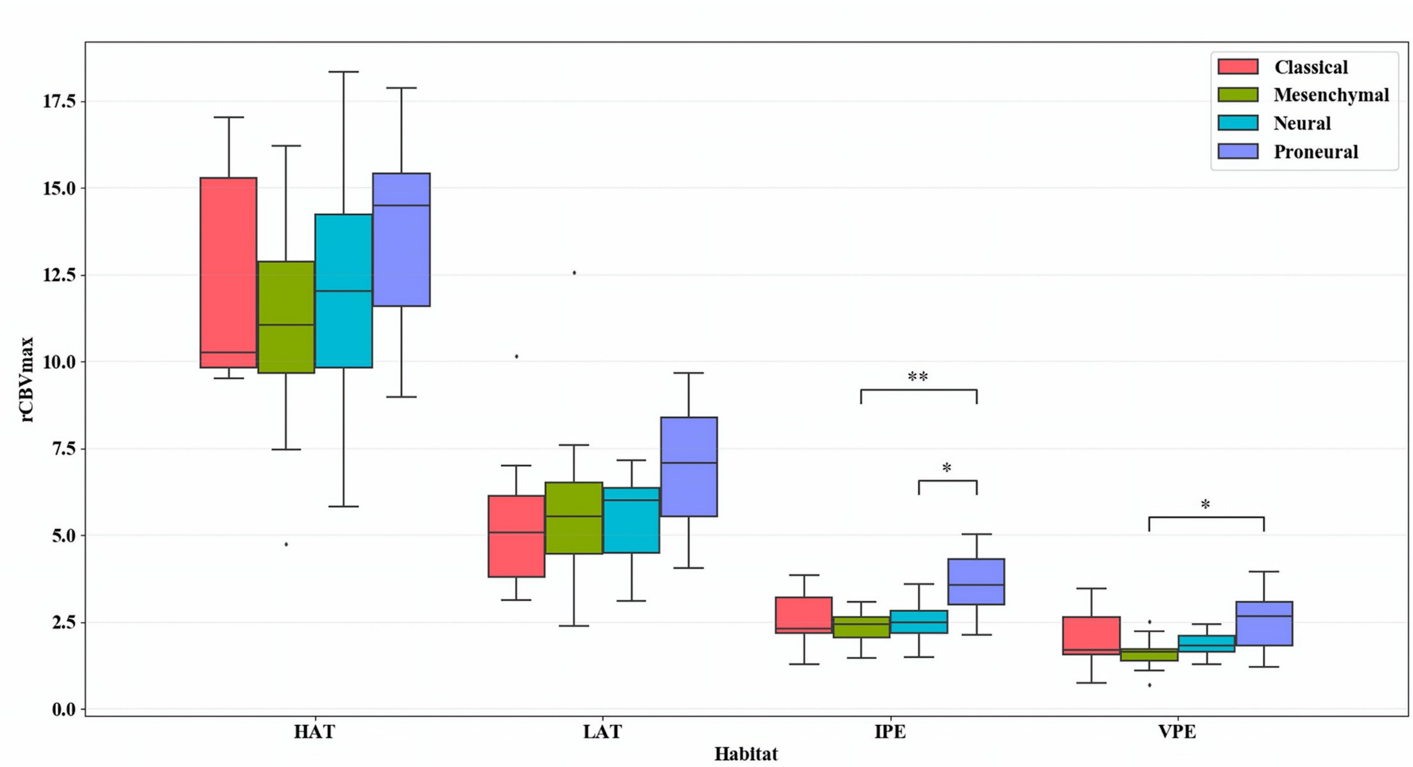

Fig 2. Box-Whiskers representation of $rCBV_{max}$ at each vascular habitat for every Verhaak subtype. Horizontal lines show the significant results of Mann-Whitney tests. * for statistical significance with $p<0.05$; ** for statistical significance with $p<0.01$; All p-values are multiple test corrected. HAT = high angiogenic tumor, LAT = low angiogenic tumor, IPE = infiltrated peripheral edema, VPE = vasogenic peripheral edema.

https://doi.org/10.1371/journal.pone.0232500.g002

were performed for the rest of habitats in the S1 Appendix, yielding only significant results for proneural against mesenchymal $rCBV_{max}$ at VPE.

When comparing proneural $rCBV_{mean}$ and $rCBV_{median}$ at IPE against the rest of the subtypes, significant differences were also found (corrected p-values of 0.0428 and 0.0420 respectively).

S1 Fig shows ROC curves for threshold optimization of the $rCBV_{max}$ at IPE using the three significant experiments after multiple test correction: (1) differentiating proneural from mesenchymal, (2) proneural from neural and (3) proneural from the of subtypes together. Optimal

Table 1. Mean and standard deviation for $rCBV_{mean}$, $rCBV_{median}$ and $rCBV_{max}$ at enhanced tumor (ET) and at infiltrated peripheral edema (IPE) habitat, and p-values from ANOVA and Kruskal-Wallis (K-W) tests in every subtype: Classical (Cla), mesenchymal (Mes), neural (Neu) and proneural (Pro).

rCBV	Region	Cla (n = 10)	Mes (n = 17)	Neu (n = 11)	Pro (n = 12)	p ANOVA	p K-W
Max	ET	8.42 ± 3.10	9.17 ± 4.24	8.85 ± 2.64	10.84 ± 2.43	0.41	0.13
	IPE	2.58 ± 0.81	2.35 ± 0.43	2.51 ± 0.57	3.60 ± 0.97	<0.001*	0.02*
Mean	ET	4.01 ± 1.74	4.14 ± 1.42	3.98 ± 0.92	5.27 ± 1.40	0.11	0.11
	IPE	1.78 ± 0.59	1.57 ± 0.31	1.76 ± 0.38	2.55 ± 0.81	<0.001*	0.03*
Median	ET	4.50 ± 1.80	4.67 ± 1.73	4.53 ± 1.07	5.79 ± 1.40	0.17	0.16
	IPE	1.83 ± 0.60	1.62 ± 0.31	1.78 ± 0.39	2.58 ± 0.78	<0.001*	0.02*

All p-values are multiple test corrected

* for statistical significance.

https://doi.org/10.1371/journal.pone.0232500.t001

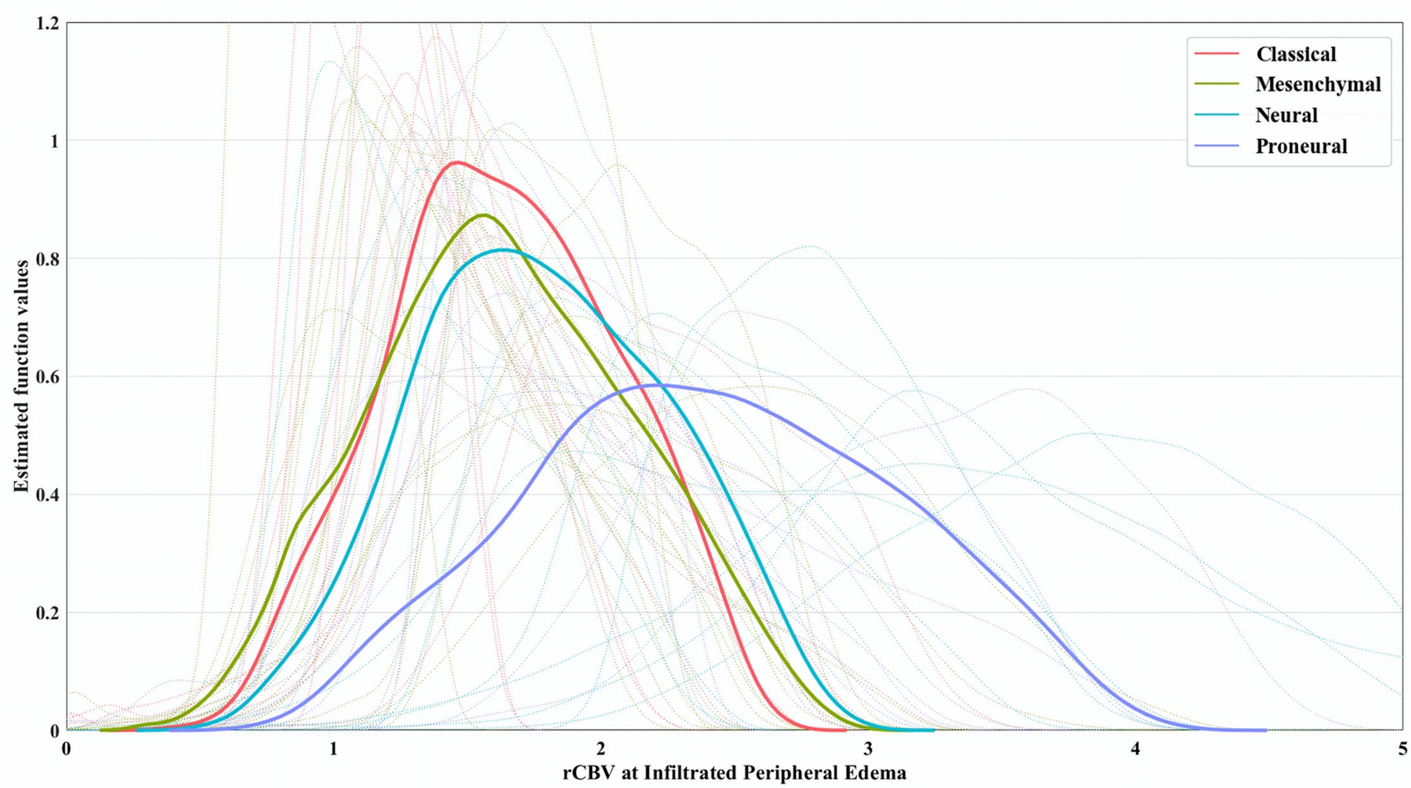

Fig 3. Kernel smoothed density distribution for rCBV values at infiltrated peripheral edema for each patient and molecular signature. Dotted lines represent density distribution for each patient. Solid lines represent the mean density distribution of patients grouped by molecular subtype.

https://doi.org/10.1371/journal.pone.0232500.g003

value for distinguishing proneural from mesenchymal was a $rCBV_{max}$ of 3.10 at IPE, whereas for proneural from neural the best cutoff was a $rCBV_{max}$ of 3.01 at IPE. Finally, the optimal threshold for differentiating proneural from the rest of Verhaak subtypes was a $rCBV_{max}$ of 3.12 at IPE.

Overall survival analysis

Table 3 shows Cox proportional hazards regression for $rCBV_{max}$ at IPE and Verhaak subtypes. Vascularity at IPE alone is significatively associated with overall survival. Proneural subtype

Table 2. Mann Whitney U-test p-values comparing rCBV values at infiltrated peripheral edema habitat in each subtype against the others individually and rCBV values of each subtype against the rest.

$rCBV_{max}$ at IPE	Classical	Mesenchymal	Neural	Proneural
Classical	1.0000	-	-	-
Mesenchymal	0.9047	1.0000	-	-
Neural	1.0000	0.7939	1.0000	-
Proneural	0.1100†	0.0043*	0.0386*	1.0000
Rest	0.9047	0.1023†	0.9047	0.0043*

All p-values are multiple test corrected

* for statistical significance after multiple test correction

† for statistical significance before multiple test correction.

https://doi.org/10.1371/journal.pone.0232500.t002

Table 3. Cox proportional hazards regression results for a total of 9 models: Uniparametric using $rCBV_{max}$ at infiltrated peripheral edema (IPE) and Verhaak subtypes and multiparametric using their combination.

	$rCBV_{max}$ at IPE		Verhaak Subtype		
	HR (CI95)	p-value	HR (CI95)	p-value	AUC
$rCBV_{max}$ at IPE	1.81 (1.2, 2.7)	0.0045*	-	-	0.5815
Classical	-	-	0.99 (0.5, 2.0)	0.9748	0.5037
Mesenchymal	-	-	0.83 (0.4, 1.6)	0.5904	0.5407
Neural	-	-	0.61 (0.3, 1.3)	0.1958	0.5403
Proneural	-	-	2.58 (1.2, 5.4)	0.0113*	0.5847
$rCBV_{max}$+ Classical	1.81 (1.2, 2.7)	0.0045*	0.97 (0.5, 2.0)	0.9469	0.5806
$rCBV_{max}$+ Mesenchymal	1.87 (1.2, 2.9)	0.0058*	1.15 (0.6, 2.4)	0.7066	0.5676
$rCBV_{max}$+ Neural	1.77 (1.2, 2.7)	0.0064*	0.65 (0.3, 1.4)	0.2741	0.5898
$rCBV_{max}$+ Proneural	1.55 (1.0, 2.5)	0.0759	1.67 (0.7, 4.1)	0.2577	0.6102

* for statistical significance.

https://doi.org/10.1371/journal.pone.0232500.t003

also yields significant results. When adding subtypes as cofactors, HR, p-values and AUC are maintained relatively stable for every subtype except proneural. In the latter, p-values escalated to non-significance and HR decreased, affecting also confidence intervals. AUC increase is no longer meaningful as neither regressor is significantly associated with survival. All of this points to a blurring in the effect of the biomarker due to the addition of correlated redundant molecular information.

The same test was performed for $rCBV_{max}$ at ET in the S2 Appendix. As a well-known biomarker, it also shows significant association with overall survival by its own. In this case, however, when adding the subtypes as cofactors, HR and significance is maintained for every subtype, including proneural, sometimes even improving AUC.

Discussion

In this study, we examined whether the vascular properties of the potentially infiltrated peripheral edema habitat were correlated with Verhaak molecular subclasses, and especially the proneural subtype. The results show that a value of $rCBV_{max}$ higher than 3.12 at IPE is significantly related to proneural subtype.

There are several studies aiming to determine the influence of genetic expression patterns in MRI features within the edema region. Carrillo *et al.* pointed out that edema could have prognostic importance in cases when *MGMT* promoter is methylated [34], which is a common trait in the proneural subtype [35]. Naeini *et al.* discovered that T2 and FLAIR volume hyperintensity representing edema was higher in proneural phenotypes [36] and Zinn *et al.* published that, by stratifying into high and low FLAIR radiophenotypes, they could identify glioblastoma subtypes [37]. Finally, the study of MRI perfusion and genetics of GBM from Barajas *et al.*, pointed out the need for a deeper understanding of peritumoral non-enhancing tumor for its risk in future progression as its genetic expression pattern differs from that of the enhancing lesion [18].

In light of these results, in this study we analyzed the radiomic relevance of the edema using a more detailed characterization of edema heterogeneity by differentiating between non-enhancing (i.e. IPE) and vasogenic edema (i.e. VPE), based on ONCOhabitats approach [15]. This allowed to overcome a limitation pointed out in previous studies [36] and thus identify the IPE as a region with a radiomic relevance when studying the proneural type. In particular, we found a significant association of the rCBV at the IPE with the glioblastoma molecular profile.

The prognosis potential of the rCBV in glioblastoma at the ET ROI has been extensively studied [14, 38, 39]. The prognosis potential of the rCBV in glioblastoma in the non-enhancing region was also suggested in some studies [15, 23, 40]. Jain *et al*. performed a survival analysis estimating HR for rCBV in both the enhancing and non-enhancing areas adjusting them for the Verhaak molecular subtypes and using the same database as this study [19]. They found that statistical significance for vascularity enhancing areas improved, suggesting additional information provided by molecular profile. However, for the edema region, it did not improve when adding the molecular information. The different molecular behavior of enhancing and non-enhancing regions is consistent with our results. Moreover, our method allowed to find bigger differences when adjusting for the proneural subtype. Thus, the Cox regression model performed in this study suggested that the predictive power of rCBV at non-enhancing areas could be related to its relationship with survival-related mutations.

As Verhaak noted when describing the molecular subclasses, they can be therapeutically relevant [5]. The fact that the biggest differences were found between the proneural and mesenchymal subtypes may point out that their vascular behavior in peritumoral regions varies broadly. As these two have been the most clinically relevant [10, 12], being able to identify them by specific perfusion features can be crucial for diagnosing and treating glioblastoma patients.

Additionally, in 2016 the WHO published a glioblastoma classification mainly differentiating whether the *IDH* gene presents itself as mutant or wild-type [2]. Our findings could also agree with the classification: the proneural subtype was the most significantly different subtype from the three remaining and it has proven to be the most closely related to *IDH1* mutations [5]. Unfortunately, not enough information was available to confirm if *IDH*-mutant vascularity at the peripheral areas was significantly different from wild-type.

Finally, in 2012 Strum *et al*. showed that the perceived better outcome for proneural subtype was caused by the presence of IDH-mutant patients and, when they were removed, proneural patients actually had the worst prognosis [41]. This is also supported by the studies that evaluated the TCGA-GBM dataset and found proneural had the shortest median survival [5, 19]. Our findings show that the proneural subtype has the highest vascularity in the peripheral edema, which could be considered a surrogate for aggressiveness.

There were some limitations in this study. Firstly, though we were able to correlate the IPE habitat and the Verhaak subclasses, due to the retrospective nature of the study, we were not able to standardize MRI acquisition protocols. Secondly, it can be difficult to correctly assess the exact location of the infiltrated edema by a noninvasive manner. These could affect the potential relationships with molecular markers. Nonetheless determining the IPE habitat by an automated method for calculating the maximum of the cerebral blood volume to perform seems robust enough for our purpose, as shown by Álvarez-Torres *et al*. [23]. Finally, despite having significant results, the sample size available in the dataset may be a statistical limitation.

Our study relies on the use of an automatic procedure to determine a more precise peritumoral ROI based on an open service [24] and the results can be replicated using the TCGA-GBM open dataset [26].

Conclusions

In conclusion, high IPE vascularity features are associated with the proneural subtype. Global vascularity differences between the four subtypes exist in this region especially due to proneural and mesenchymal influence. $rCBV_{max}$ at IPE is related to overall survival and carries specific molecular information.

Supporting information

S1 Table. Clinical data of the final cohort. All clinical data is obtained from the TCGA-GBM open database [26]. Subtype and genetic information were retrieved from the UCSC Xena platform compilation [28] which is based on Brennan *et al* [27] (Supplementary Material 9).
(XLSX)

S2 Table. MRI scanners and protocols used for each subject.
(XLSX)

S3 Table. $rCBV_{max}$, $rCBV_{mean}$ and $rCBV_{median}$ at every habitat for each subject.
(XLSX)

S1 Appendix. Mann Whitney U-test comparing $rCBV_{max}$ at each habitat for Verhaak subtypes.
(DOCX)

S2 Appendix. Cox proportional hazards regression for $rCBV_{max}$ at ET and Verhaak subtypes.
(DOCX)

S1 Fig. ROC curves for $rCBV_{max}$ at IPE threshold optimization for significant experiments. Significant experiments: distinguishing proneural from mesenchymal, proneural from neural and proneural from the rest.
(TIF)

Acknowledgments

We gratefully acknowledge the COST Association for its CA18206—Glioma MR Imaging 2.0 European project which supports the research on glioblastoma.

Author Contributions

Conceptualization: Eduard Chelebian, Elies Fuster-Garcia, Juan M. García-Gómez.

Investigation: Eduard Chelebian.

Methodology: Eduard Chelebian, Javier Juan-Albarracín.

Software: Javier Juan-Albarracín.

Supervision: Elies Fuster-Garcia, Juan M. García-Gómez.

Validation: María del Mar Álvarez-Torres.

Writing – original draft: Eduard Chelebian.

Writing – review & editing: Elies Fuster-Garcia, María del Mar Álvarez-Torres, Juan M. García-Gómez.

References

1. Louis DN, Ohgaki H, Wiestler OD, Cavenee WK, Burger PC, Jouvet A, et al. The 2007 WHO Classification of Tumours of the Central Nervous System. *Acta Neuropathol* 2007; 114(2):97–109 https://doi.org/10.1007/s00401-007-0243-4 PMID: 17618441
2. Louis DN, Perry A, Reifenberger G, von Deimling A, Figarella-Branger D, Cavenee WK, et al. The 2016 World Health Organization Classification of Tumors of the Central Nervous System: a summary. *Acta Neuropathol* 2016; 131(6):803–820 https://doi.org/10.1007/s00401-016-1545-1 PMID: 27157931

3. Bai H, Harmancı AS, Erson-Omay EZ, Li J, Coşkun S, Simon M, et al. Integrated genomic characterization of IDH1-mutant glioma malignant progression. *Nat Genet* 2015; 48(1):59–66 https://doi.org/10.1038/ng.3457 PMID: 26618343
4. Chen JR, Yao Y, Xu HZ, Qin ZY. Isocitrate Dehydrogenase (IDH)1/2 Mutations as Prognostic Markers in Patients with Glioblastomas. *Medicine* 2016; 95(9) e2583 https://doi.org/10.1097/MD.0000000000002583 PMID: 26945349
5. Verhaak RGW, Hoadley KA, Purdom E, Wang V, Qi Y, Wilkerson MD, et al. Integrated Genomic Analysis Identifies Clinically Relevant Subtypes of Glioblastoma Characterized by Abnormalities in PDGFRA, IDH1, EGFR, and NF1. *Cancer Cell* 2010; 17(1):98–110 https://doi.org/10.1016/j.ccr.2009.12.020 PMID: 20129251
6. Turcan S, Rohle D, Goenka A, Walsh LA, Fang F, Yilmaz E, et al. IDH1 mutation is sufficient to establish the glioma hypermethylator phenotype. *Nature* 2012; 483(7390):479–483 https://doi.org/10.1038/nature10866 PMID: 22343889
7. He ZC, Ping YF, Xu SL, Lin Y, Yu SC, Kung HF et al. Lower MGMT expression predicts better prognosis in proneural-like glioblastoma. *Int J Clin Exp Med* 2015; 8(11):20287–20294 PMID: 26884942
8. Cooper LAD, Gutman DA, Long Q, Johnson BA, Cholleti SR, Kurc T, et al. The Proneural Molecular Signature Is Enriched in Oligodendrogliomas and Predicts Improved Survival among Diffuse Gliomas. *PLoS One* 2010; 5(9):e12548 https://doi.org/10.1371/journal.pone.0012548 PMID: 20838435
9. Sandmann T, Bourgon R, Garcia J, Li C, Cloughesy T, Chinot OL, et al. Patients with Proneural Glioblastoma May Derive Overall Survival Benefit from the Addition of Bevacizumab to First-Line Radiotherapy and Temozolomide: Retrospective Analysis of the AVAglio Trial. *J Clin Oncol* 2015; 33(25):2735–2744 https://doi.org/10.1200/JCO.2015.61.5005 PMID: 26124478
10. Fedele M, Cerchia L, Pegoraro S, Sgarra R, Manfioletti G. Proneural-Mesenchymal Transition: Phenotypic Plasticity to Acquire Multitherapy Resistance in Glioblastoma. *Int J Mol Sci* 2019; 20(11):2746
11. Olar A, Aldape KD. Using the molecular classification of glioblastoma to inform personalized treatment. *J Pathol* 2013; 232(2):165–177
12. Behnan J, Finocchiaro G, Hanna G. The landscape of the mesenchymal signature in brain tumours. *Brain* 2019; 142(4):847–866 https://doi.org/10.1093/brain/awz044 PMID: 30946477
13. Law M, Young RJ, Babb JS, Peccerelli N, Chheang S, Gruber ML, et al. Gliomas: Predicting Time to Progression or Survival with Cerebral Blood Volume Measurements at Dynamic Susceptibility-weighted Contrast-enhanced Perfusion MR Imaging. *Radiology* 2008; 247(2):490–498 https://doi.org/10.1148/radiol.2472070898 PMID: 18349315
14. Hirai T, Murakami R, Nakamura H, Kitajima M, Fukuoka H, Sasao A, et al. Prognostic Value of Perfusion MR Imaging of High-Grade Astrocytomas: Long-Term Follow-Up Study. *AJNR Am J Neuroradiol* 2008; 29(8):1505–1510 https://doi.org/10.3174/ajnr.A1121 PMID: 18556364
15. Juan-Albarracín J, Fuster-Garcia E, Pérez-Girbés A, Aparici-Robles F, Alberich-Bayarri Á, Revert-Ventura A, et al. Glioblastoma: Vascular Habitats Detected at Preoperative Dynamic Susceptibility-weighted Contrast-enhanced Perfusion MR Imaging Predict Survival. *Radiology* 2018; 287(3):944–954 https://doi.org/10.1148/radiol.2017170845 PMID: 29357274
16. Tan W, Xiong J, Huang W, Wu J, Zhan S, Geng D. Noninvasively detecting Isocitrate dehydrogenase 1 gene status in astrocytoma by dynamic susceptibility contrast MRI. *J Magn Reson Imaging* 2017; 45:492–9 https://doi.org/10.1002/jmri.25358 PMID: 27367599
17. Hempel J-M, Schittenhelm J, Klose U, Bender B, Bier G, Skardelly M, et al. In Vivo Molecular Profiling of Human Glioma. *Clin Neuroradiol* 2018; 29(3):479–491 https://doi.org/10.1007/s00062-018-0676-2 PMID: 29468261
18. Barajas RF Jr, Hodgson JG, Chang JS, Vandenberg SR, Yeh R-F, Parsa AT, et al. Glioblastoma Multiforme Regional Genetic and Cellular Expression Patterns: Influence on Anatomic and Physiologic MR Imaging. *Radiology* 2010; 254(2):564–576 https://doi.org/10.1148/radiol.09090663 PMID: 20093527
19. Jain R, Poisson L, Narang J, Gutman D, Scarpace L, Hwang SN, et al. Genomic Mapping and Survival Prediction in Glioblastoma: Molecular Subclassification Strengthened by Hemodynamic Imaging Biomarkers. *Radiology* 2013; 267(1):212–220 https://doi.org/10.1148/radiol.12120846 PMID: 23238158
20. Ryoo I, Choi SH, Kim J-H, Sohn C-H, Kim SC, Shin HS, et al. Cerebral Blood Volume Calculated by Dynamic Susceptibility Contrast-Enhanced Perfusion MR Imaging: Preliminary Correlation Study with Glioblastoma Genetic Profiles. *PLoS One* 2013; 8(8):e71704 https://doi.org/10.1371/journal.pone.0071704 PMID: 23977117
21. Gill BJ, Pisapia DJ, Malone HR, Goldstein H, Lei L, Sonabend A, et al. MRI-localized biopsies reveal subtype-specific differences in molecular and cellular composition at the margins of glioblastoma. *Proc Natl Acad Sci USA* 2014; 111(34):12550–12555 https://doi.org/10.1073/pnas.1405839111 PMID: 25114226

22. Price SJ, Young AMH, Scotton WJ, Ching J, Mohsen LA, Boonzaier NR, et al. Multimodal MRI can identify perfusion and metabolic changes in the invasive margin of glioblastomas. *J Magn Reson Imaging* 2015; 43(2):487–494 https://doi.org/10.1002/jmri.24996 PMID: 26140696

23. Álvarez-Torres M del M, Juan-Albarracín J, Fuster-Garcia E, Bellvís-Bataller F, Lorente D, Reynés G, et al. Robust association between vascular habitats and patient prognosis in glioblastoma: An international multicenter study. *J Magn Reson Imaging* https://doi.org/10.1002/jmri.26958 PMID: 31654541

24. Juan-Albarracín J, Fuster-Garcia E, García-Ferrando GA, García-Gómez JM. ONCOhabitats: A system for glioblastoma heterogeneity assessment through MRI. *Int J Med Inform* 2019 Aug; 128:53–61 https://doi.org/10.1016/j.ijmedinf.2019.05.002 PMID: 31160012

25. Juan-Albarracín J, Fuster-Garcia E, Manjón JV, Robles M, Aparici F, Martí-Bonmatí L, et al. Automated Glioblastoma Segmentation Based on a Multiparametric Structured Unsupervised Classification. *PloS One* 2015; 10(5): e0125143 https://doi.org/10.1371/journal.pone.0125143 PMID: 25978453

26. Scarpace L, Mikkelsen T, Cha S, Rao S, Tekchandani S, Gutman D, et al. Radiology Data from The Cancer Genome Atlas Glioblastoma Multiforme [TCGA-GBM] collection [Data set]. *The Cancer Imaging Archive* 2016. Available from: https://wiki.cancerimagingarchive.net/display/Public/TCGA-GBM

27. Brennan CW, Verhaak RGW, McKenna A, Campos B, Noushmehr H, Salama SR, et al. The Somatic Genomic Landscape of Glioblastoma. *Cell* 2013 Oct; 155(2):462–77 https://doi.org/10.1016/j.cell.2013.09.034 PMID: 24120142

28. Goldman M, Craft B, Hastie M, Repečka K, Kamath A, McDade F, et al. The UCSC Xena platform for public and private cancer genomics data visualization and interpretation. *Cold Spring Harbor Laboratory* 2018.

29. Boxerman JL, Schmainda KM, Weisskoff RM. Relative Cerebral Blood Volume Maps Corrected for Contrast Agent Extravasation Significantly Correlate with Glioma Tumor Grade, Whereas Uncorrected Maps Do Not. *AJNR Am J Neuroradiol* 2006 Apr; 27(4):859–867 PMID: 16611779

30. Juan-Albarracín J, Fuster-Garcia E, del Mar Álvarez-Torres M, Chelebian E, García-Gómez JM. ONCOhabitats Glioma Segmentation Model. In: *Brainlesion*: *Glioma*, *Multiple Sclerosis*, *Stroke and Traumatic Brain Injuries*. Springer International Publishing; 2020. p. 295–303.

31. Javier Juan-Albarracín, Elies Fuster-Garcia, Alfons Juan and Juan M. García-Gómez. Non-Local Spatially Varying Finite Mixture Models for Image Segmentation. *Stat*. *Comput* 2020. Accepted for publication.

32. Guo L, Wang G, Feng Y, Yu T, Guo Y, Bai X, et al. Diffusion and perfusion weighted magnetic resonance imaging for tumor volume definition in radiotherapy of brain tumors. *Radiat Oncol*. 2016 Sep 21; 11(1).

33. R Core Team (2020). R: A language and environment for statistical computing. R Foundation for Statistical Computing, Vienna, Austria. https://www.R-project.org/

34. Carrillo JA, Lai A, Nghiemphu PL, Kim HJ, Phillips HS, Kharbanda S, et al. Relationship between Tumor Enhancement, Edema, IDH1 Mutational Status, MGMT Promoter Methylation, and Survival in Glioblastoma. *AJNR Am J Neuroradiol* 2012; 33(7):1349–1355 https://doi.org/10.3174/ajnr.A2950 PMID: 22322613

35. Noushmehr H, Weisenberger DJ, Diefes K, Phillips HS, Pujara K, Berman BP, et al. Identification of a CpG Island Methylator Phenotype that Defines a Distinct Subgroup of Glioma. *Cancer Cell* 2010; 17 (5), 510–522 https://doi.org/10.1016/j.ccr.2010.03.017 PMID: 20399149

36. Naeini KM, Pope WB, Cloughesy TF, Harris RJ, Lai A, Eskin A, et al. Identifying the mesenchymal molecular subtype of glioblastoma using quantitative volumetric analysis of anatomic magnetic resonance images. *Neuro Oncol* 2013; 15(5):626–634 https://doi.org/10.1093/neuonc/not008 PMID: 23444259

37. Zinn PO, Majadan B, Sathyan P, Singh SK, Majumder S, Jolesz FA, et al. Radiogenomic Mapping of Edema/Cellular Invasion MRI-Phenotypes in Glioblastoma Multiforme. *PLoS One* 2012; 7(2)

38. Romano A, Pasquini L, Di Napoli A, Tavanti F, Boellis A, Rossi Espagnet MC, et al. Prediction of survival in patients affected by glioblastoma: histogram analysis of perfusion MRI. *J Neuro Oncol* 2018; 139(2):455–460

39. Fuster-Garcia E, Juan-Albarracín J, García-Ferrando GA, Martí-Bonmatí L, Aparici-Robles F, García-Gómez JM. Improving the estimation of prognosis for glioblastoma patients by MR based hemodynamic tissue signatures. *NMR Biomed* 2018; 31(12)

40. Jain R, Poisson LM, Gutman D, Scarpace L, Hwang SN, Holder CA, et al. Outcome Prediction in Patients with Glioblastoma by Using Imaging, Clinical, and Genomic Biomarkers: Focus on the Nonenhancing Component of the Tumor. *Radiology* 2014; 272(2):484–493 https://doi.org/10.1148/radiol.14131691 PMID: 24646147

41. Sturm D, Witt H, Hovestadt V, Khuong-Quang D-A, Jones DTW, Konermann C, et al. Hotspot Mutations in H3F3A and IDH1 Define Distinct Epigenetic and Biological Subgroups of Glioblastoma. *Cancer Cell* 2012 Oct; 22(4):425–37. https://doi.org/10.1016/j.ccr.2012.08.024 PMID: 23079654